

A novel computational model for the analysis of contra-rotating propellers

Vít Štorch^{1,*}, Jiří Nožička¹

¹ Czech Technical University in Prague, Faculty of Mechanical Engineering, Department of Fluid Dynamics and Thermodynamics, Technická 4, 166 07 Praha 6, Czech Republic

Abstract

Following the work concerning single rotating propeller the paper extends the theory successfully applied and verified for simple scenario of a single propeller to a more challenging case of two coaxial contra-rotating propellers. The described method is based on a force-free unsteady wake formed by a vortex sheet which is connected to a lifting line representing the propeller blade. These basic elements that are also used for the single propeller simulation case need to be modified to remove the strong singularities present when vortex sheets intersect, or when the lifting line of the second propeller passes through the wake of the first propeller.

Key words: Contra-rotating propellers, lifting line theory, blade loading, force-free wake, vortex sheet

1. Introduction

There are many different approaches to designing an aircraft propeller. The key aspect of the computational model is the prediction of induced velocity at the propeller plane. The methods for evaluation of induced velocity are usually based on the vortex wake theory, which under some assumptions and simplifications can lead to analytical solution. In general, however, a numerical procedure, either steady or unsteady, is needed for the correct computation of induced velocity and propeller loading.

A computational model that uses a lifting line positioned at $1/4$ of chord along the blade span and a force free wake system consisting of vortex filaments has been developed and used for analysis and design of small aircraft propellers.

The goal of current work is extending the computational model to be able to handle the case of two contra-rotating coaxial propellers.

The contra rotating propellers appearing sporadically in experimental and single-purpose aircraft as early as in the pre WWII era were designed using simple analytical approaches. Even the large and powerful contra-rotating propellers of the TU-95 aircraft produced in larger numbers were designed in 1950s well before the wide spread of numerical methods fueled by growing amount of computational power available. Nowadays, there are basically two different emerging applications for contra-rotating propellers. For low speed and low budget applications such as drones, the presented method is a perfect solution in terms of ease of use, precision of results and computational time required. Another type of application is the high power, high speed operation of modern transport aircraft (Fig. 1). A suitable approach for designing and fine-tuning these propellers lies in modern RANS CFD solvers, capable of handling all of the flow physics including dissipation, sound generation and compressibility effects. Even in these circumstances the presented method could

provide a good initial design point for further optimization using commercial software.



*Fig. 1. 3DR X8 quadcopter with contra-rotating propellers
Source: <http://diydrones.com>*

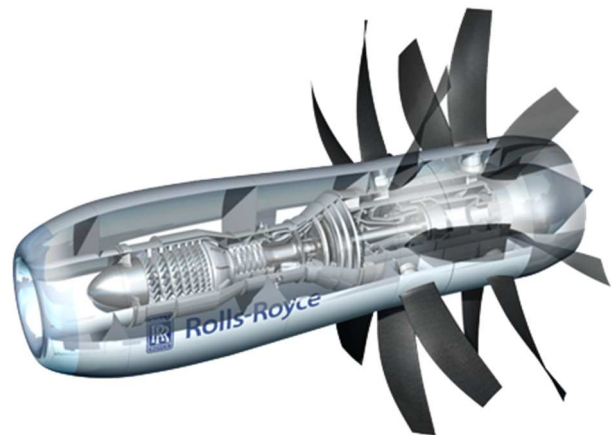


Fig. 2. Roll-Royce Open rotor technology. Source: <http://www.rolls-royce.com>

* Corresponding author, Vit.Storch@fs.cvut.cz

2. Basic elements of the model

The computational model is a natural expansion and continuation of the previous work focused on single propellers [1]. The whole process of calculation is automated using scripts and functions written in MATLAB. One section of the MATLAB code also runs the separate XFOIL executable, an aerodynamic tool written by M. Drela for low Reynolds number airfoil analysis [2].

Each rotor can contain an arbitrary number of blades. Each of the propeller blades is modeled separately, without using any kind of symmetry, due to the fact that oncoming airflow can have an off-axis direction, which is common especially during flight of multi-copter drones.

The blade is discretized into N equidistant span stations (Fig. 3). Each span station is characterized by the airfoil geometry, incidence (twist) angle, chord length and sweep position. Based on the rate of rotation, a Reynolds number is estimated for each span station and the aerodynamic polar is computed for each airfoil with appropriate Re using XFOIL.

Each span station contains a starting element of a horseshoe vortex forming the lifting line connecting the $1/4$ chord positions of all airfoil sections. First segment of the vortex wake sheet behind the lifting line connecting the $1/4$ chord and trailing edge is fixed (red color, Fig. 3) the rest of the wake behaves as a force free wake.

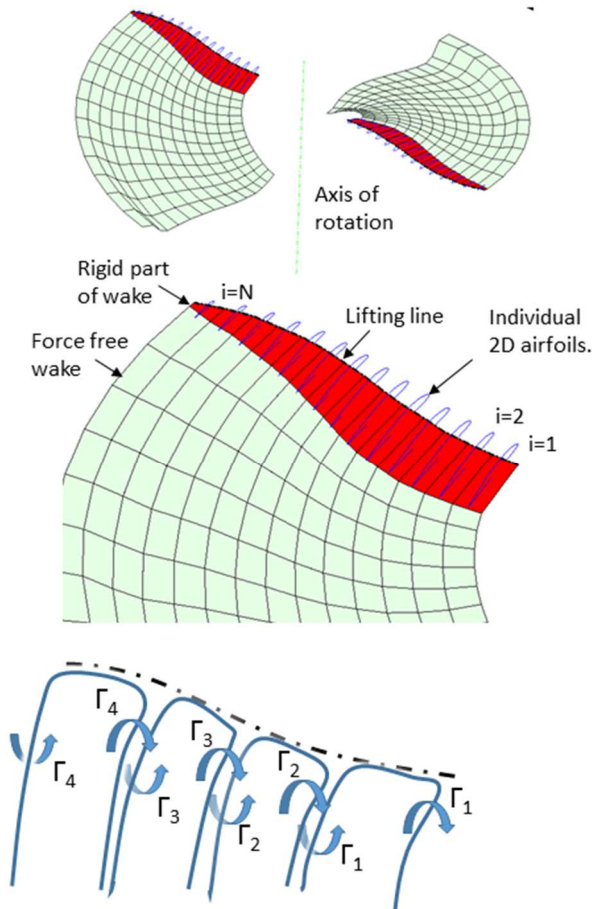


Fig. 3. Basic components of the computational model

2.1. Circulation on the lifting line

The polars of each airfoil at respective span stations are stored in a tabular format as lift and drag coefficients at different angles of attack.

$$c_l = c_l(\alpha) \quad (1)$$

$$c_d = c_d(\alpha) \quad (2)$$

For calculating the circulation at span station i , the free stream velocity \vec{v}_∞ (which may have any direction), the relative velocity \vec{v}_{rel} due to rotation and induced velocity \vec{v}_i from the wake system add to form the total relative velocity \vec{v} . The angle of attack α is then the angle between the chord line and projected velocity vector \vec{v}' (the oncoming velocity \vec{v} projected into the plane of airfoil section). The circulation is computed as follows:

$$\Gamma = \frac{1}{2} c_l c |\vec{v}'| \quad (3)$$

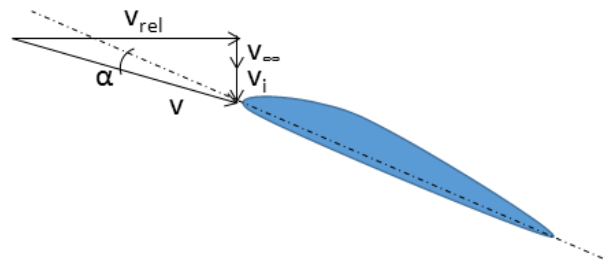


Fig. 4. The total relative velocity as the sum of its components

2.2. Vortex wake

The vortex shedding at the trailing edge is a direct result of the Helmholtz's second theorem and Kutta condition applied to the trailing edge. The lifting line just as any other vortex filament cannot end in fluid and has to continue into the wake. To be able to represent various circulation distributions, the vortex shedding does not occur only at the blade tips, but also between each span station. The Helmholtz's first theorem states, that vortex filament must be constant. For steady case, the wake can be built of infinitely long horseshoe vortices. For unsteady case, it is necessary to use vortex rings as the basic element for construction of the wake. Each vortex ring retains the circulation of the lifting line at the time it was shed. By observing the changing circulation of the wake panels (rings) heading downstream we can obtain the time history of the circulation of the lifting line (Fig.6).

In order to reduce computation resources it is a good practice to combine the segments of the neighboring vortex rings into one vortex filament which has the net circulation obtained by subtracting the circulations of the neighboring vortex rings. This way, the total number of vortex segments reduces almost two times which can bring up to four times shorter calculation of geometric influence coefficients.

The geometric influence coefficients of a vortex filament are in its basic form three components U_{ij} , V_{ij} , W_{ij} , of velocity that j -th filament of unit circulation induces at

a specific point P_i in space. (Fig.5). The matter was covered in more detail in previous work [3] concerning 3D panel methods.

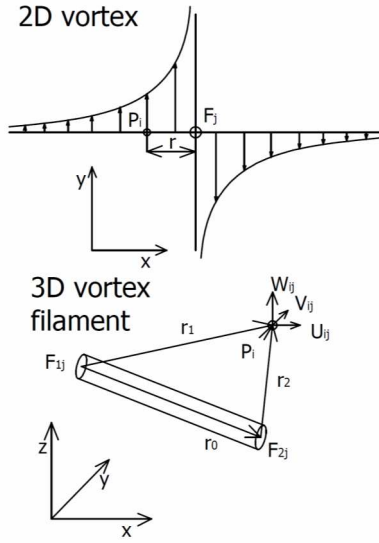


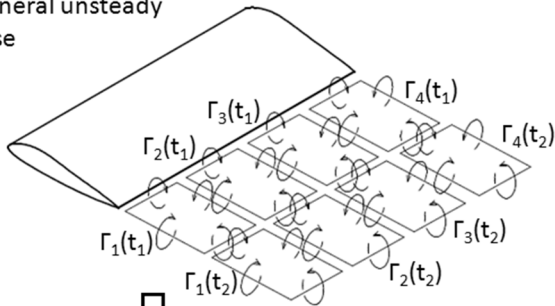
Fig. 5. The 2D vortex with velocity field, 3D vortex filament F_j and its induced velocity at random point P_i .

The geometric coefficients are calculated as follows with circulation $\Gamma=1$ [4]:

$$[U_{ij}, V_{ij}, W_{ij}] = \frac{\Gamma}{4\pi} \frac{\vec{r}_1 \times \vec{r}_2}{|\vec{r}_1 \times \vec{r}_2|^2} \vec{r}_0 \left(\frac{\vec{r}_1}{|\vec{r}_1|} - \frac{\vec{r}_2}{|\vec{r}_2|} \right) \quad (4)$$

Note that the 3D vortex filament suffers naturally with the same singularity as the 2D vortex. As the point P_i approaches the filament, the cross product of the vectors \vec{r}_1 and \vec{r}_2 approaches zero since the angle between vectors approaches 180° and the induced velocity goes to infinity.

General unsteady case



Steady case
 $\Gamma_i(t_1) = \Gamma_i(t_2) = \text{const}$

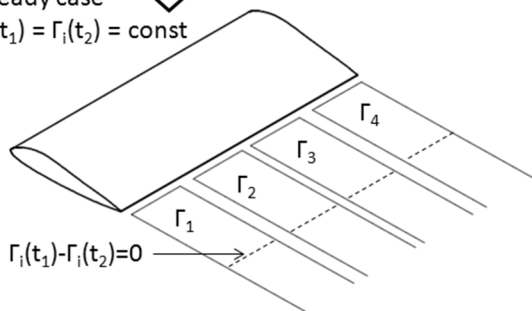


Fig. 6. The unsteady vortex wake and its simplification for steady case.

2.3. Wake kinematics

The inertial coordinate system was chosen as the reference frame for all the calculations. Each time step $t_i = t_{i-1} + \Delta t$, the blades are rotated in their prescribed direction by an angle $\varphi_i = \varphi_i + \Omega \Delta t$. All the nodes of the force-free wake move in the direction of absolute velocity obtained as a sum of free stream and induced velocities at the node (Fig.7). New position of node with coordinates $\vec{P}(t)$ is expressed as:

$$\vec{P}(t_i) = \vec{P}(t_{i-1}) + (\vec{v}_\infty + \vec{v}_i) \Delta t \quad (5)$$

The gap, which appears between the rigid wake and force-free wake after each time step is filled with a new row of vortex rings, which are assigned the appropriate circulation from current lifting line circulation distribution.

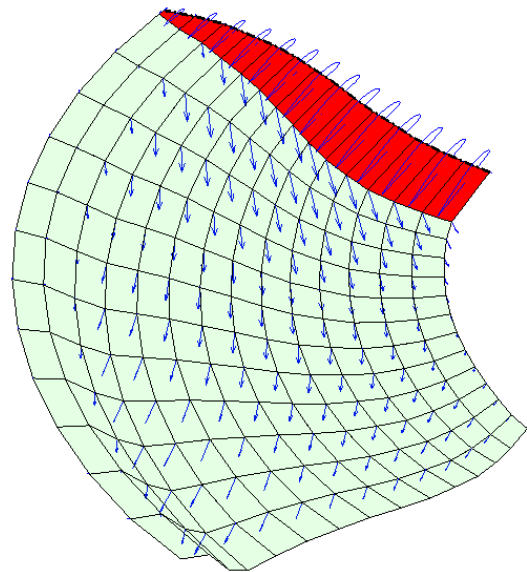


Fig. 7. The force free wake with absolute velocity at each node, which determines the direction and amount of displacement during next time step.

2.4. Unsteady solution algorithm

The solver time marching solution of the basic computational model, able to handle the single propeller case can be described in a few simple steps.

During initialization, only the rigid part of the wake and single row of force-free wake are created. All the starting circulations are considered to be zero, so during first iteration step, there are no induced velocities.

As the first step, the angle of attack and relative velocity magnitude are calculated. Since there is zero induced velocity at the beginning, the angle of attack will be relatively high, usually greater than the maximum angle of attack computed by XFOIL. The computed polars must be therefore artificially extended to provide at least some data also in the fully stalled regime.

In the second step, the blades are rotated and vortex wake moved as described in the wake kinematics. Newly

shed wake panels (rings) inherit the lifting line circulations and the induced velocities are calculated at wake nodes and lifting line nodes. It is assumed, that the velocity at a node lying directly on a vortex filament induced by this very same filament is zero. This procedure repeats in a loop, each pass providing solution at specific time. This means that there is only one iteration per time step.

The whole process is equivalent to a propeller starting its rotation from a full stop and accelerating to full speed within one time step (i.e. instantly). Several full revolutions are needed before the wake develops its shape and correct induced velocities are calculated.

2.5. Example of the use of unsteady model for single rotor calculation.

The model described in previous paragraphs suffers from some inherent issues when used on a more complex case, such as vertical axis turbine. The most prominent issue is the non-physical induced velocity of nodal points in close proximity of wake, which happens when a wake intersects itself, another wake or the lifting line or a body modeled by 3D panel surface. The issue has been partially solved in previous work [5] by limiting the maximum induced velocity near a filament which is in fact the simplest vortex core model.

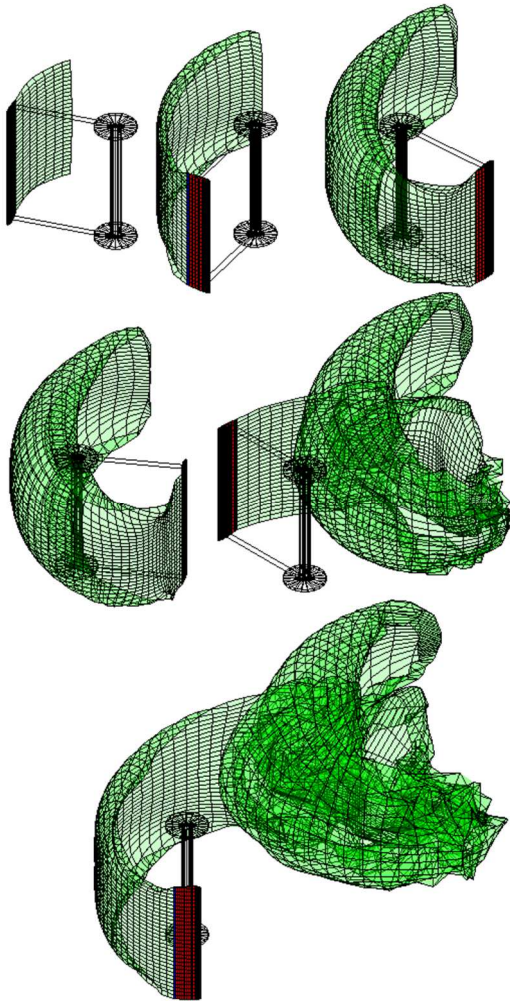


Fig. 8. The unsteady vortex wake development behind a single blade of vertical axis turbine. Described in [5].

3. Model for contra-rotating propellers

There are several reasons, why the basic model described in previous section fails to provide solution for a setup of contra-rotating propellers. Moreover, there are several areas where the model can be improved even for the calculation of single propellers. These aspect will be addressed in order of importance in the following sections.

3.1. Vortex core model

One approach to removing singularities near vortex ring sheet is a local tessellation scheme that interpolates velocity at surface collocation points and points in sufficient distance from the surface as suggested by Dixon et al. [6] Vortex core model is an important tool for handling singularity near the vortex filament.

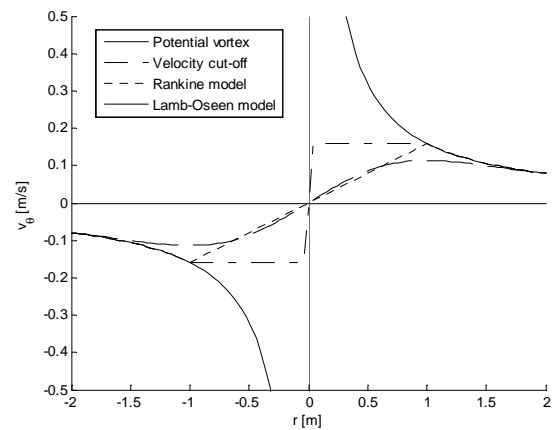


Fig. 9. The tangential velocity in the vicinity of a 2D vortex of unit strength. Vortex core is set to 1 m.

For the described computation, Lamb-Oseen [7] core model was chosen, and modified to provide functionality for calculation of induced velocity of 3D vortex filament as follows:

$$[U_{ij}, V_{ij}, W_{ij}] = \frac{\Gamma}{4\pi} \frac{\vec{r}_1 \times \vec{r}_2}{|\vec{r}_1 \times \vec{r}_2|^2} \vec{r}_0 \left(\frac{\vec{r}_1}{|\vec{r}_1|} - \frac{\vec{r}_2}{|\vec{r}_2|} \right) (1 - e^q) \quad (6)$$

Where:

$$q = -1.25643 \left(\frac{|\vec{r}_1 \times \vec{r}_2|^2}{r_c |\vec{r}_0|^2} \right) \quad (7)$$

The size of the vortex core is selected to be lower than the distance between vortex filaments. This way, the core model doesn't affect the solution of a single propeller, only enhances and in fact makes possible the simulation of the second rotor.

3.2. Relaxation and modified iteration scheme

Since the circulation of the lifting line depends strongly on induced velocity and this induced velocity depends through the presence of the first vortex ring row on the lifting line circulation, there is always a danger of the solution becoming unstable. In the case of single propeller,

where the flow conditions seen by the rotor blade become eventually steady, it is possible to include simple relaxation scheme, where new circulation is constructed partly from equation (3) and partly from the previous time step circulation. This process is not possible for contra-rotating propellers, because the second propeller blades are subject to ever changing flow conditions and circulation distribution needs to react instantly to this change. The current solution is to insert several iteration steps with relaxation for each time step, in such a way, that no circulation from previous time step is used for constructing the new time step circulation. This solution can be still unstable especially when the blade is discretized by large number of span stations and it adds to the overall computational time. Several other solutions will be tried in the future work to increase the stability and decrease the computational cost of this relaxation procedure.

3.3. Initial wake blow off at static operation

During static operation, the free stream velocity is zero or close to zero. When the computation starts in such conditions, the propeller is subject to large angles of attack due to low induced velocity from the short wake. The initial wake circulations are as a result far from the values of developed solution. Since there is very low absolute velocity at the wake nodes, the wake has a tendency to “linger” close to the propeller, before the induced velocities rise up. By that time the initial portion of wake is stretched, deformed and influencing the flow conditions at the propeller.

The following procedure has been developed, which is used for low advance coefficients and at static conditions. An artificial free stream velocity is provided during initialization, which linearly decreases to the required free stream velocity during time-marching. This can be described as blowing off the wake during propeller start. It must be ensured that the artificial component of free stream velocity disappears well before the end of iterations.

Another measure that may be useful is the decay of the vorticity in the wake which will be handled in the future versions of the model.

3.4. First results

As the experimental data are yet to be measured the model was tested with the data of a random propeller PT 22x10E3 intended for single prop use. The same type of two bladed propeller (second propeller is only mirrored) was used for the first and second rotor of a contra-rotating system. The example data were prepared with distance between propellers 0.2 diameters and both propellers rotating at the same angular velocity, only in opposite direction. The advance ratio of axial velocity to tip speed was chosen quite low $\lambda=0.05$, to demonstrate the wake blow-off ability. The thrust coefficient c_t of each blade can be calculated as follows:

$$c_t = \frac{\sum_2^1 \rho c_l c v^2 \Delta R}{\rho \left(\frac{\Omega}{2\pi}\right)^2 D^2} \quad (8)$$

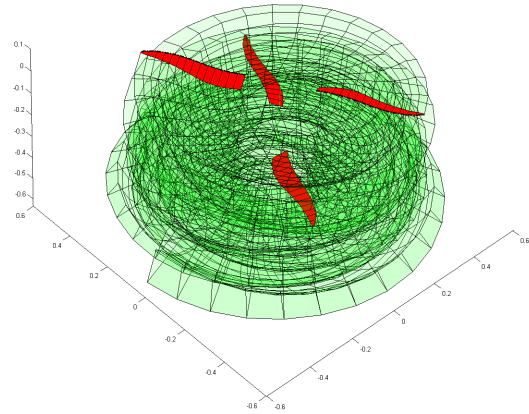


Fig. 10. The wake of a contra-rotating set of propellers in axial free-stream velocity field

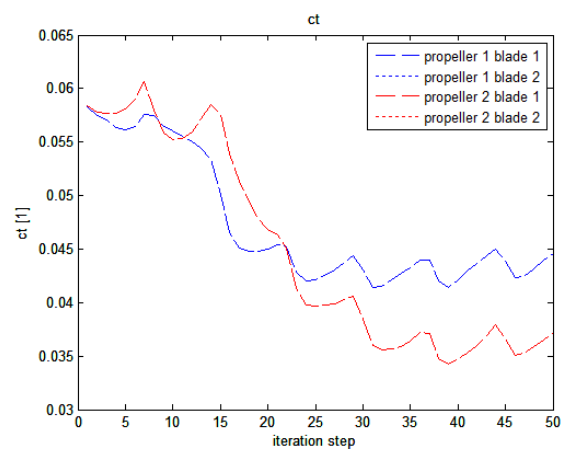


Fig. 11. The time history of thrust coefficient of each blade

It can be noted that the second propeller is more lightly loaded and that it takes roughly two revolutions for the solution to stabilize. Also, the curves of thrust coefficient for both blade of each propeller lie on top of each other, since the flow is axisymmetric.

For the second test case, the free stream velocity is given an x -component of the same magnitude as the axial (z) velocity. The freestream flow direction now forms an angle of 45° with the axis.

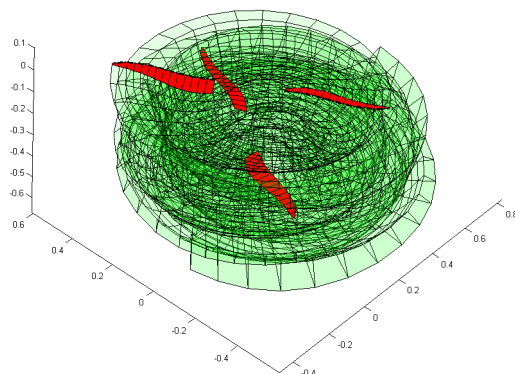


Fig. 12. The wake of a contra-rotating set of propellers in general inclined free-stream velocity field

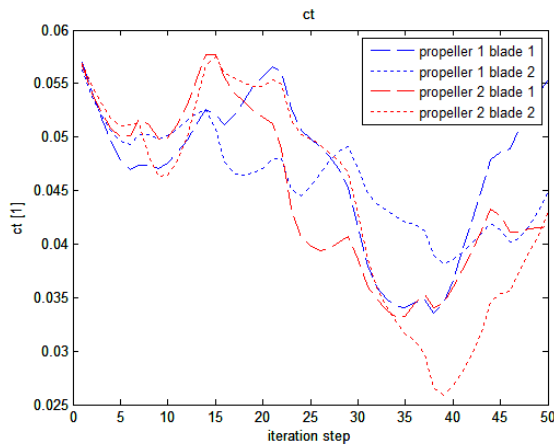


Fig. 13. The time history of thrust coefficient of each blade under inclined free stream velocity field.

3. Conclusion

The presented unsteady computational model for analysis of contra-rotating propellers in an arbitrary flow field is by no means finished. It is important to obtain precise and reliable experimental data for validation. When performing validation, there are several possibilities for fine-tuning the method according to experiment. After vortex core growth and decay model is added, visualization and velocity measurement in the wake may provide some information about the behavior of vortex structures in the wake.

The computational model will be useful for very fast sensitivity studies that should reveal the effects of angular speed, diameter and pitch ratios of the two propellers as well as the influence of the propeller distance. It can also provide an interesting insight into the operation of the contra-rotating propeller in a free stream coming from the side, which is equivalent to a regular flight regime of the drones.

List of symbols

c	chord length (m)
c_l	lift coefficient (1)
c_t	thrust coefficient (1)
D	Propeller diameter (m)
\vec{P}_i	radius vector of point P (m)
\vec{R}_i	radius of the lifting line span station
$\vec{r}_{1,2,0}$	radius vectors for calculation of geometric coefficients (m)
Δt	time step (s)
\vec{v}	relative velocity (m/s)
\vec{v}_i	induced velocity (m/s)
\vec{v}_∞	free stream velocity (1)
U_{ij}	x-component of geometric coefficient (m/s)
V_{ij}	y-component of geometric coefficient (m/s)
W_{ij}	z-component of geometric coefficient (m/s)
α	angle of attack ($^\circ$)
ρ	density ($\text{kg}\cdot\text{m}^{-3}$)
Ω	angular velocity (rad/s)

Γ	circulation (m^2/s)
φ	position angle of the propeller ($^\circ$)

References

- [1] FILIPSKÝ, J., ŠTORCH, V. *Comparison of propeller analysis methods and experimental data*. In *Engineering Mechanics 2014*. Brno: Brno University of Technology, 2014, p. 172-175. ISBN 978-80-214-4871-1.
- [2] DRELA M. *XFOIL: An Analysis and Design System for Low Reynolds Number Airfoils*, Low Reynolds Number Aerodynamics, Springer-Verlag Lec. Notes, 1989
- [3] ŠTORCH, V., NOŽIČKA, J. *3D panel methods for turbomachinery design*. In: *Studentská tvůrčí činnost 2014*. Praha: České vysoké učení technické v Praze, Fakulta strojní, 2014, ISBN 978-80-01-05484-0.
- [4] KATZ J., Plotkin A. *Low-Speed Aerodynamics*. Cambridge Aerospace Series. Cambridge University Press, 2001. ISBN 9780521665520.
- [5] ŠTORCH, V., NOŽIČKA, J. BRADA, M. SUCHÝ, J. *Experimental Verification of Computational Model for Wind Turbine Blade Geometry Design*. In *EFM14 - Experimental Fluid Mechanics 2014*. Liberec: Technical University of Liberec, 2015, p. 572-577. ISSN 2100-014X
- [6] DIXON, K., SIMAO FERREIRA, C.J., HOFEMAN, C., VAN BUSSEL, G.J.W., VAN KUIK, G.A.M. *A 3d unsteady panel method for vertical axis wind turbines* In: *The proceedings of the European Wind Energy Conference & Exhibition EWEC Brussels*, European Wind Energy Association EWEA, 2008
- [7] SAFFMAN P. G., ABLOWITZ, M J., J. HINCH, E., OCKENDON, J. R., OLVER, P. J., *Vortex Dynamics*. Cambridge University Press, 1992.

Acknowledgements: This work was supported by the Grant Agency of the Czech Technical University in Prague, grant No. SGS16/068/OHK2/1T/12